Fermi National Accelerator Laboratory

FERMILAB-Pub-97/379-E
E868, APEX

A Detector to Search for Antiproton Decay at the Fermilab Antiproton Accumulator

T. Armstrong et al.
The APEX Collaboration

Fermi National Accelerator Laboratory
P.O. Box 500, Batavia, Illinois 60510

December 1997

Submitted to *Nuclear Instruments and Methods in Physics Research Section A*

Operated by Universities Research Association Inc. under Contract No. DE-AC02-76CH03000 with the United States Department of Energy

Disclaimer

Distribution

FERMILAB-Pub-97/379-E

A Detector to Search for Antiproton Decay at the Fermilab Antiproton Accumulator

T. Armstrong [e], C. Buchanan [a], B. Corbin [a], S. Geer [b], R. Gustafson [c], M. Hu [d], M. Lindgren [a], J. Marriner [b], M. Martens [b], T. Muller [a,1], R. Ray [b], A. Scott [a], G.R. Snow [d,2], J. Streets [b], W. Wester [b]

[a] *University of California at Los Angeles, Los Angeles, California 90024, USA*

[b] *Fermi National Accelerator Laboratory, Batavia, Illinois 60510, USA*

[c] *University of Michigan, Ann Arbor, Michigan 48109, USA*

[d] *University of Nebraska–Lincoln, Lincoln, Nebraska 68588, USA*

[e] *Pennsylvania State University, University Park, Pennsylvania 16802, USA*

(The APEX Collaboration)

We describe the experimental apparatus used by the APEX experiment (Experiment 868) at the Fermilab Antiproton Accumulator. The experiment is designed to search for decays of 8.9 GeV/c antiprotons as they traverse a 3.7 m long evacuated decay tank inserted in a straight section of the Antiproton Accumulator ring. The detector components in the experimental set-up are discussed individually, and the performance of the experiment during data-taking is described.

PACS codes: 11.30.Er, 14.20Dh, 13.30.Ce, 07.07.-a

Keywords: Antimatter, Antiproton, CPT, Detector, Fermilab, Proton

Submitted to Nuclear Instruments and Methods in Physics Research, Section A

[1] Present address: Universität Karlsruhe, 76128 Karlsruhe, Germany

[2] Corresponding author. Tel. +1 402 472 6279, email gsnow@unlhep.unl.edu, gregsnow@fnald0.fnal.gov

1 Introduction

The APEX experiment was designed to search for antiproton ($\overline{p}$) decay at the Fermilab Antiproton Accumulator. The CPT theorem requires that the antiproton lifetime ($\tau_{\overline{p}}$) be equal to the proton lifetime (τ_p). Previous and ongoing searches for proton decay indicate that $\tau_p > O(10^{32})$ years [1]. The APEX experiment searches for $\overline{p}$ decay with a lifetime $\tau_{\overline{p}} << O(10^{32})$ years, and therefore provides a test of the CPT theorem.

The most sensitive laboratory search for inclusive $\overline{p}$ decay was performed using a Penning trap to store of order 1000 $\overline{p}$s produced in the Low Energy Antiproton Ring at CERN. This experiment yielded the result [2] that $\tau_{\overline{p}} > 0.28$ years. Greater sensitivity can be achieved by exploiting the intense source of antiprotons provided by the Fermilab Antiproton Accumulator and searching for exclusive decay modes of the antiproton. Angular momentum conservation requires that there be a fermion in the final state, and hence the simplest candidate $\overline{p}$ decay modes are two-body final states containing an electron, a negative muon, or a neutrino. The APEX test experiment (Fermilab experiment T861), which was designed to explore the feasibility of searching for exclusive decays of the antiproton at Fermilab Antiproton Accumulator, yielded limits on the lifetime divided by branching ratio ($\tau_{\overline{p}}$ /B.R.) for five modes with an electron in the final state. The most stringent of these limits was $\tau_{\overline{p}}\ /B.R. > 1848$ years [3] for the decay mode $\overline{p} \rightarrow e^- + \gamma$.

Following the success of the T861 experiment, the APEX experiment (Fermilab experiment 868) was designed to improve on the sensitivity of the test experiment by about a factor of 1000 and to cover a greater variety of candidate decay modes. The APEX experiment searches for decays of the circulating 8.9 GeV/c antiprotons as they traverse a 3.7 m long evacuated decay tank installed in a straight section of the Accumulator ring. The detector is designed to search for $\overline{p}$ decay modes which contain an electron in the final state: $\bar{p} \rightarrow e^- + X$ where $X = \gamma, \pi^0, \eta, K^0_S$, etc. Final states which include a muon instead of an electron are also studied. With an average of 10^{12} $\overline{p}$s (corresponding to 100 mA beam current) stored in the Accumulator, the experiment collected data from April to July in 1995. A measure of the sensitivity of this data sample is given by:

$$S = \frac{1}{\gamma_{\overline{p}}} \int N_{\overline{p}}(t)\, dt = 3.31 \times 10^9\, years,$$

where $N_{\overline{p}}(t)$ is the number of circulating antiprotons at time t, $\gamma_{\overline{p}} = 9.5$ is the Lorentz factor for the 8.9 GeV/c $\overline{p}$s, and the integral is over the live-time of the experiment. Hence, if $\tau_{\overline{p}} = 3.31 \times 10^9$ years then on average one $\overline{p}$ decay would have occurred somewhere within the Accumulator during the live-time of the experiment.

2 Experimental Layout

Fig. 1 shows a side view of the APEX detector. It is located in a 15.9 m straight section in the Accumulator ring, which has a circumference of 474 m. Antiprotons entering from the left traverse a 3.7 m long evacuated decay tank operated at 10^{-11} Torr. The downstream section of the tank consists of a 96 cm diameter cylinder with a 1.2 mm thick stainless steel window. Upstream of the tank, 4 horizontal and 4 vertical scintillation counters are arranged around the 10 cm diameter beam pipe in a 1×1 m^2 plane to veto tracks from upstream interactions. At the upstream end of the tank is a movable tungsten wire target which can be inserted into the antiproton beam halo to create particles for calibrating the detector.

Particles emerging from the decay region within the tank encounter planes of scintillation counters used for triggering, planes of scintillating fibers for tracking, a pre-radiator, and an electromagnetic calorimeter [4]. Between the pre-radiator and the calorimeter are planes of horizontal and vertical proportional tubes. Behind the calorimeter is a 20 cm deep lead wall followed by horizontal and vertical planes of scintillation counters which serve as a tail catcher (TC). The TC strengthens the experiment's electron and photon identification, since electromagnetic shower particles should be completely absorbed by the calorimeter (14.7 radiation lengths) and the TC lead (35.7 radiation lengths), with no particles reaching the TC scintillators. Finally, a limited-acceptance muon telescope, 10 nuclear interaction lengths in depth, is located behind the tail catcher. The muon telescope is a sandwich of iron plates and scintillation counters used to search for $\overline{p}$ decay modes which contain a muon. The individual detector elements are described in detail in the following sections.

The upstream part of the APEX apparatus, from the vacuum tank through the proportional tubes, is located over a 4.4 m long pit whose bottom is 91 cm below the normal Accumulator floor and 165 cm below the $\overline{p}$ beam. The calorimeter, tail catcher and muon telescope are downstream of the pit and rest on the Accumulator floor 74 cm below the $\overline{p}$ beam. Cables of length $\approx$70 m carry signals from the detectors to the experiment's counting room.

3 Vacuum Tank

The APEX vacuum tank replaces a section of the normal Accumulator beam pipe upstream of the APEX detector. It provides a high-vacuum decay volume to minimize background events from $\overline{p}$ beam-gas interactions. The tank is constructed from 304 stainless steel and provides a 3.7 m long conical evacuated

fiducial volume with a full opening angle of 12.8°. The downstream end of the tank is a closed by a 1.2 mm thick stainless steel window with a diameter of 96 cm. The thickness of the window was chosen to minimize the material (7.3% radiation length) encountered by particles exiting the decay volume toward the detectors, whilst maintaining the mechanical integrity under vacuum.

The vacuum system was designed to achieve pressures of 1×10^{-11} Torr or better. The vacuum system consists of a 400 l/s ion pump and twelve titanium sublimation filaments. A layer of titanium covering 1.2 m^2 is sublimated directly on the inside of the vacuum tank, providing an estimated pumping speed of 3.2×10^4 l/s for hydrogen. To reduce outgassing from the tank walls the different sections of the vacuum tank were vacuum degassed prior to final assembly by baking at 950 $°C$ for 2 hours at a vacuum of 1×10^{-4} Torr. After installation the tank was also baked in situ for 48 hours at a temperature of 280 $°C$.

Two nude Bayard-Alpert vacuum ionization gauges [5] were installed to measure the pressure in the tank. In addition, a residual gas analyzer (RGA) [6] was used to measure the partial pressures of the individual gas species. The ion gauges are sensitive to pressures as low as 1×10^{-11} Torr while the RGA is sensitive to partial pressures as low as 1×10^{-15} Torr. The vacuum ultimately achieved was approximately 1×10^{-11} Torr which is 10 times better than the vacuum in the rest of the Accumulator ring. The residual gas was predominantly H_2 with CH_4, H_2O, CO, CO_2 and Ar contributing about 1% each in partial pressure. At a pressure of 1.0×10^{-11} Torr the residual proton and neutron densities were 1.7×10^6 cm^{-3} and 1.1×10^6 cm^{-3}, respectively.

The APEX experiment was designed to run parasitically, and not to adversely affect normal Accumulator operation. It was therefore important that the beam impedance of the vacuum tank was not large enough to create microwave instabilities which cause beam loss. For the beam conditions in the Accumulator, instabilities are predicted if the tank impedance Z/n is larger than 850 Ω [7], where Z is the impedance of the tank cavity mode and n is the cavity mode frequency divided by the revolution frequency of the Accumulator. Modeling the tank as a cylindrically symmetric cavity the 2-dimensional code URMEL [8] was used to calculate the frequencies and impedances of the cavity modes. The highest Z/n value was 450 Ω. Although this is below the instability threshold, 4 passive RF damping loops were installed as an added precaution to reduce the largest Z/n to 230 Ω.

Negatively charged clearing electrodes were installed in the tank to attract and remove positive ions created by $\overline{p}$s colliding with residual gas molecules. At sufficiently high densities, such ions could interact coherently with the $\overline{p}$ beam and create instabilities [9]. The voltage and geometry of the electrodes must produce potential minima at their locations so that the ions do not collect

elsewhere in the tank. A 3-dimensional finite element code, OPERA-3d [10], was used to verify that placing the clearing electrodes at the upstream and downstream ends of the tank would be sufficient to remove trapped ions. As expected, no instabilities were observed in the Accumulator with the vacuum tank installed.

3.1 Movable target

A movable 0.28 mm diameter tungsten wire target was installed at the upstream end of the vacuum tank to help calibrate the APEX detector. The target rests below from the $\overline{p}$ beam during normal data-taking. For special calibration runs, a stepping motor could move the target upward into the beam halo to provide a localized source of particle interactions. The target-in position was determined by moving the wire into the halo until the trigger rates increased by a factor of 10 over the target-out position.

4 Electromagnetic Calorimeter

APEX used the forward electromagnetic (e.m.) calorimeter of the E760 experiment previously run at the Fermilab Antiproton Accumulator. This calorimeter is described in detail in [4]. The calorimeter is a lead/scintillator sampling device which consists of 144 rectangular modules arranged in a 13 $\times$ 13 array, as shown in Fig. 2, with six modules removed from each of the four corners. One module at the center is removed to allow for the Accumulator beam pipe.

Each calorimeter module consists of 148 alternate layers of lead plates and acrylic scintillator tiles [11] with transverse dimensions of 10 $\times$ 10 cm^2. The lead plates are 1 mm thick. The first 32 scintillator tiles are 0.64 cm thick, the last 42 tiles are alternately 0.64 cm and 0.32 cm thick, and each tile is wrapped with 25 μm aluminum foil. The calorimeter presents a total of 14.7 radiation lengths of absorber (Pb/scintillator/Al) to normally incident particles.

The light generated in the scintillator tiles of each module is read out with a single wavelength-shifting (WLS) plate [12] placed along one side of the module (Fig. 2). The 0.64 cm thick WLS plate covers the full 10 cm height and 48 cm depth of the module and extends 3 cm beyond the back. Light emerging from the back of the WLS plate is transmitted through an adiabatic lucite light-guide and a lucite disk to a 5.1 cm diameter photomultiplier tube (PMT) [13] directly behind the module. Attached to the lucite disk is an optical fiber which leads to an LED pulser system used to monitor the relative gain of the PMTs. With the modules stacked as in Fig. 2, about 10% of the surface area

of the calorimeter face is insensitive (absorber-less) due to the WLS plates and the wrapping materials around each module. The analog outputs from the PMTs were digitized by a CAMAC-based, charge-sensitive 11-bit Lecroy ADC system [14] located in the experimental counting room (Sec. 8.2).

4.1 Calorimeter Calibration

The calorimeter was calibrated in situ using data collected with special triggers. The position dependence of the module response was mapped out using data collected with a trigger based on the veto counters (Sec. 6.2) and the calorimeter tail catcher (Sec. 4.2), located upstream and downstream of the calorimeter. These counters selected particles originating far upstream of the experiment which passed through the full depth of the calorimeter at approximately normal incidence. Offline, the scintillating-fiber tracking system (Sec. 5.1) was used to determine the impact points of these particles on the face of a given module with a precision of $\approx$1 mm.

Fig. 3 shows the mean pulse height as a function of perpendicular distance away from the WLS plate for particles incident on nine adjacent 1 cm wide vertical slices on the face of a typical calorimeter module. The response is steeply attenuated over the first few cm away from the WLS plate, while the attenuation is more shallow over the last few cm. The curve in Fig. 3 is a fit to the data points using a function which is the sum of a constant plus an exponential. This pulse-height attenuation is attributed to geometric effects in the light collection in the scintillator tiles and ageing of the scintillator over time. The attenuation did not appear to be due to accumulated radiation exposure, since the attenuation characteristics did not depend on the position of the modules relative to the $\overline{p}$ beam. Fig. 4 shows the pulse-height distributions for two of the vertical slices centered (a) 2.5 cm away from the edge of the WLS plate and (b) 5.5 cm away. The peak in (b) is attenuated by 64% relative to (a), and the fractional width in (b) is larger than in (a). The position-dependent response and resolution functions derived from this study were built into the GEANT [15] model of the calorimeter. The dashed curves in Figs. 4a and 4b are obtained from GEANT simulations of the energy deposited in the scintillator planes for 5 GeV charged pions incident on the module and match the data well.

The calorimeter energy scale was established using $\pi^0 \rightarrow \gamma\gamma$ decays produced during target-in calibration runs. To measure the energies and position centroids of e.m. showers, a clustering algorithm was developed which incorporated the position-dependent module responses described above. Fig. 5 shows invariant mass distributions for two-cluster events with successive cuts applied to enhance the π^0 peak. The effectiveness of the scintillating fiber tracker (Sec.

5.1) and the pre-radiator counters (Sec. 6.1) is seen in the middle and bottom plots. Target-in calibration runs were taken periodically during the experiment and time-dependent calibration constants were introduced to center the reconstructed π^0 mass on its known value.

Fig. 6 shows two-cluster invariant mass distributions in the region of (a) the π^0 peak and (b) the η peak. The π^0 plot shows a Gaussian fit to the data which has a fractional rms width of 25%. The η plot shows a fit which is the sum of a Gaussian (fractional width 22%) and a polynomial representing the combinatoric background. The fractional width of the π^0 peak is roughly 30% larger than that quoted in [4] using a similar technique for π^0 reconstruction. The apparent degradation of the energy resolution is attributed to the ageing of the calorimeter over time.

4.2 Tail Catcher

Behind the e.m. calorimeter is a tail catcher (TC) which consists of a 20 cm thick lead wall followed by two planes of NE110 [16] polystyrene scintillation counters. The tail catcher (TC) strengthens the experiment's electron and photon identification, since e.m. shower particles should be completely absorbed by the calorimeter (14.7 radiation lengths) and the TC lead (35.7 radiation lengths), with no particles reaching the TC scintillators.

The TC wall was made from $5 \times 10 \times 20$ cm^3 lead bricks stacked so that there were no straight-through cracks. The wall has transverse dimensions 1.35×1.35 m^2, slightly larger than the size of the calorimeter and the TC scintillators. A 10×10 cm^2 hole at the center of the wall allows the beam pipe to pass.

Fig. 7 shows the layout of the TC scintillators. A plane of 14 horizontal counters is followed by a plane of 14 vertical counters. Each plane has ten 8.2 cm wide counters, two 10.0 cm wide counters and two 18.1 cm wide counters. The narrow counters are 1.27 cm thick, and the two wider counter sizes are 1.91 cm thick. Light is read out from one end of each counter via a lucite light guide and a 3.8 cm diameter 10-stage PMT [17]. In the experimental counting room the TC analog signals were passively split and routed to both trigger discriminators and ADC modules [18].

The TC scintillation counters were calibrated before installation using cosmic rays. The PMT high voltages were adjusted so that the mean pulse height for cosmic rays passing through the center of a counter would fall about 100 counts above the ADC pedestal. Light attenuation in the counters was also studied using cosmic-rays incident at ten positions along the length of the counters. The 8.23 and 10.0 cm wide counters had attenuation lengths of about 200 cm,

while the 18.1 cm wide counters had attenuation lengths of about 340 cm.

5 Tracking

5.1 Scintillating Fiber Tracking

Three stations of scintillating-fiber detectors provide charged-particle tracking in the APEX experiment. The longitudinal positions of the stations are indicated in Fig. 1. Each station consists of one horizontal and one vertical plane of fibers, and each plane is made of two independent L-shaped modules. Fig. 8a is a schematic of one L-shaped module and the two multi-channel PMTs which view the light from the fibers. The L-shaped design provides a 10×10 cm^2 hole for the beam pipe when two modules are oriented with PMTs facing opposite directions, as shown in Fig. 8b.

Each L-shaped module has 75 short and 309 long 2 mm diameter polystyrene scintillating fibers [19] with fiducial lengths 40 cm and 90 cm, respectively. Each fiber is 20-30 cm longer than the fiducial length, the extra length being used to route the fiber to its PMT. The core material of the fibers has an index of refraction (n) of 1.67. Each fiber has a 60 μm thick cladding with n = 1.40 and a thin coating of white reflecting paint along its length. The ends of the fibers opposite the PMT are covered with aluminized mylar to reflect light. The fibers are arranged in two staggered layers, as shown in Fig. 8c, with an average center-to-center spacing of 2.6 mm within each layer. The fibers are epoxied to a 3 mm thick L-shaped lucite panel reinforced with an aluminum bar running along the long side of the L. Each L-shaped module is covered with opaque black paper to eliminate light leaks. The fibers were measured to yield about 9 photoelectrons for a minimum-ionizing traversing charged particle, and to have a light attenuation length of about 3 m.

Two multi-channel, 12-stage Hamamatsu PMTs [20] view the fibers from each module, as shown in Fig. 8a. The 192 fibers viewed by each PMT are routed through a positioning jig which holds the fiber ends flush against the 7.6×7.6 cm^2 borosilicate window of the PMT. The jig, which is made of two parallel lucite plates with precision-drilled holes for the fibers, insures that the fibers are perpendicular to the PMT window and properly centered over the venetian-blind dynode structures in the tube. The electron avalanches are sensed by an array consisting of 24 wires (gain $\approx 6 \times 10^5$) and 8 perpendicular strips (gain $\approx 1 \times 10^6$). Each of the 192 fibers corresponds to a unique anode pair in the 32-channel analog read-out for a tube.

Mounted on the PMT bases are preamplifiers which send inverted analog

signals along 350 ns long cables to the counting room. There the signals are inverted again using passive ferrite-core inverters and fed to the same Lecroy ADC system [14] used for the calorimeter.

A track-finding algorithm was developed which combined hit information in the fiber tracker with clusters found in the e.m. calorimeter. The algorithm looped through all permutations of x and y points in the tracker, looking for combinations that pointed to clusters in the calorimeter on the downstream end of the track. Here, x (y) designates the horizontal (vertical) coordinate transverse to the beam, with z as the $\overline{p}$ beam axis. The algorithm allowed only one track to point to each candidate cluster in the calorimeter, with priority given to tracks having the highest number of data points, the lowest χ^2 for a straight-line fit and the best match to the centroid of the calorimeter cluster. For events with a single charged track, the vertex was defined to be the point at which the charged track most closely approached the $\overline{p}$ beam. For events with multiple charged tracks, the vertex was defined as the point along z where the transverse deviation of the tracks from their mean was a minimum.

The single-hit efficiency for each L-shaped panel was measured to range from 53% to 99%, with an average single-hit efficiency of 85%. This translates to a position-dependent track reconstruction efficiency which varies from 85% to 95%.

Target-in runs were used to evaluate the tracker performance, since $\overline{p}$–target interactions created tracks with a known origin. Constraining reconstructed tracks to pass through the target position, a plot of track residuals (fit position - actual fiber position) for a typical fiber plane (Fig. 9a) shows an rms width of 620 μm. Removing the constraint provided by the target position from the track fits, the z position of the target could be reconstructed with a resolution of about 13 cm (Fig. 9b). For such tracks, the reconstructed impact parameter at the target z position was typically less than about 1 cm (Fig. 9c). The tracker hit efficiencies and resolutions were built into the GEANT simulation of the tracker performance.

5.2 Proportional Tube Tracking

Between the pre-radiator and the e.m. calorimeter are planes of proportional tubes, one plane of vertical tubes followed by one plane of horizontal tubes. Each proportional-tube cell consists of a hollow aluminum extrusion, with a cross section of approximately 24 mm^2 and length of 1.5 m, which acts as the cathode. The anode is a 51 μm diameter gold-plated tungsten wire which runs down the center of the cell. The ends of the cells are closed with inserts which suspend the wires and have connections for gas flow. Eight such cells were

extruded as a single unit. The external walls are 1.8 mm thick, and the walls separating the cells are 2.0 mm thick. Each proportional-tube plane consists of seven adjacent 8-tube units, leading to 56 vertical and 56 horizontal channels. To allow for the beam pipe, four tubes at the center of each plane have a 10 cm long segment removed. The anode wires in the two remaining pieces of the segmented tubes are connected together with an insulated wire which runs around the pipe.

The tubes are filled with a gas mixture of 20% CO_2 in argon, and all wires are operated at the same high voltage, typically +2040 V. This yields a gas gain of approximately 5×10^3. The proportional-tube readout system is described in detail in [21].

6 Scintillation Counters

6.1 dE/dx counters

Three identical stations of dE/dx scintillation counters were used for triggering and for selecting events with a single charged track. The longitudinal positions of these counters are shown in Fig. 1. Four identical counters are used in each station, two oriented horizontally and two vertically, as shown in Fig. 10, allowing room for the beam to pass. Each Pilot-F scintillator has dimensions $50 \times 100 \times 1.27$ cm^3. Lucite light guides are glued to each 50 cm end and terminate in a 11.4 cm diameter lucite disk. The outer face of the disk is machined with a concave shape to match the curvature of the convex face of a RCA-8854 14-stage PMT. The analog signals from the PMTs are split and routed to discriminators for triggering and a Lecroy ADC system [14] for pulse-height digitization.

The light generated by cosmic rays incident normal to the scintillator surface was used to calibrate the dE/dx counters and study their uniformity of response. Operating voltages were determined by equalizing the means of the minimum-ionizing pulse-height distributions from the individual PMTs for cosmic rays passing through the center of each counter. Fitting the pulse-height distributions for cosmic rays incident at several positions over the face of the counters revealed a light attenuation length of about 1 m along the 1 m length of the central axis. The analog sum of the pulse heights from the two ends of the counters, however, was approximately independent of position. Hence, the two-end analog sum was discriminated for triggering purposes.

Fig. 11 shows the summed pulse height distribution from the two ends of a dE/dx counter for a sample of events in which a single charged track was

found by the scintillating fiber tracker. This minimum-ionizing distribution was tuned in the experiment's GEANT simulation routine by generating energy deposition in the scintillator according to a Landau distribution and smearing with the appropriate photostatistics. The solid curve in Fig. 11 shows the simulated distribution using a mean of 37 photoelectrons per minimum-ionizing particle (m.i.p.) for the sum of the two PMTs.

The third station of the dE/dx counters is preceded by a 1.27 cm thick lead radiator (2.3 radiation lengths) so that it serves as a pre-radiator before the e.m. calorimeter. The lead radiator is made from two 0.64 cm thick sheets, each sheet cut in half vertically. A 10 cm diameter semicircular hole in each half allows the radiator pieces to close around the beam pipe. Signals from the pre-radiator counters proved effective in the selection of e.m. showers, as shown for example in Sec. 4.1.

6.2 Veto counters

The veto counters were designed to identify particles originating upstream of the decay volume. They are located 8 cm upstream of the movable target, as shown in Fig. 1. A plane of vertically-oriented counters is followed by an identical plane of horizontal counters. Each plane consists of 4 scintillators measuring $25 \times 100 \times 0.8$ cm^3 arranged to cover a 1×1 m^2 area. In each plane, the two counters nearest the beam pipe have a semicircular cut-out to accommodate the pipe. A lucite light guide and a PMT are attached to one end of each counter.

The analog signals from the veto counters are discriminated using thresholds below that expected for minimum-ionizing particles, and the 'OR' of the 8 discriminated signals is used in anti-coincidence with most of the triggers described in Sec. 8.1.

7 Muon Telescope

A simple muon detector was placed behind the e.m. calorimeter and the tail catcher to explore the feasibility of studying $\overline{p}$ decay modes which contain a muon. The muon telescope, shown in Fig. 12, is a sandwich of 5 identical sections of iron absorber followed by scintillator planes. Each iron module, made of 6 identical plates stacked in depth, measures $30.5 \times 30.5 \times 30.3$ cm^3 which provides 2 nuclear interaction lengths per module. Each scintillator plane is $30 \times 30 \times 1.91$ cm^3. The muon telescope is supported by a steel frame which points its central axis toward the center of the 3.7 m long decay

volume. The muon telescope intercepts 1.5% of the solid angle in the $\overline{p}$ rest frame for decays which would occur at the center of the decay volume.

Decay muons from the process $\overline{p} \rightarrow \mu^- + \gamma$ occurring at the center of the decay tank would have an energy ranging between 2 and 8 GeV at the muon telescope. Muons in this range deposit approximately 105 MeV in the e.m. calorimeter, 254 MeV in the tail catcher and 1700 MeV in the muon telescope. Multiple Coulomb scattering in the iron of the telescope will cause many muons in the above energy range to be deflected by a few cm as they penetrate, so some muons are expected to scatter out of the telescope before the last scintillator plane.

The scintillator planes were calibrated before installation using the pulse heights from minimum-ionizing cosmic rays incident at their centers. During the experiment, online muon triggers required at least two scintillator planes to have coincident signals above a minimum-ionizing threshold. Offline muon identification is more restrictive, requiring 4 or 5 planes above threshold.

8 Triggering and Data Acquisition

8.1 Triggering

Triggers were developed to select events which might result from antiproton decay. The e.m. calorimeter, the dE/dx counters and the muon detector were used in different combinations for various final state particles and event topologies. To aid with electron and photon selection, the analog signals from the blocks in four quadrants of the calorimeter, shown in Fig. 13 as $Q_1, ..., Q_4$, were summed. A calorimeter E_{total} signal was also formed using the analog sum of all 144 blocks. The 8 blocks surrounding the $\overline{p}$ beam were operated with lowered gains so that they would not contribute to the trigger sums.

Three types of triggers were implemented for decay modes resulting in e.m. energy deposition in the calorimeter. The first, $E_{balance}$, capitalized on the transverse-momentum balance of two-body decays and required energy in diagonally opposite calorimeter quadrants above an adjustable threshold. The second was aimed at multi-particle decay modes and required E_{total} to be above an adjustable threshold. The third was an electron trigger which required hits in the scintillators of the 3 dE/dx planes corresponding to a particular calorimeter quadrant with energy over threshold. For the electron trigger, the pre-radiator dE/dx counters were required to have energy deposition greater than that expected for one m.i.p.

For decay modes containing a muon, a muon trigger required energy deposition in at least two of the scintillators in the muon telescope. In each of the above triggers, the veto counters were used in anti-coincidence to eliminate events with particles originating upstream of the decay volume.

The following trigger rates were typical for a data-taking run with a $\overline{p}$ current of 100 mA: 3 Hz for $E_{balance}$, 9 Hz for E_{total}, 8 Hz for the electron trigger, and 1 Hz for the muon trigger.

8.2 Data Acquisition

The APEX detectors were read out from five CAMAC crates on a parallel branch highway into a VAX3200 via a Jorway 411 branch highway QBUS interface. There were approximately 1000 ADC channels and 50 TDC channels read with VAXONLINE [22]. All data were zero suppressed, and a typical event length was 730 bytes. Separate event records containing information from the accelerator complex were read from the ACNET system [23] and written with the main data to 8 mm tape. The ACNET records included readings of the $\overline{p}$ beam current, beam emittances, pressures in the decay tank and the beam pipe near the APEX apparatus, and the status of the lithium lens near the $\overline{p}$ source which indicated whether $\overline{p}$ stacking was in progress. Buffers of events were sent from the VAX3200 to an SGI Indigo R4000 over ethernet for online histogramming and 3D event display.

The event rate was limited to 100 Hz due to the 10 ms VAX interrupt and readout time. Runs with a typical $\overline{p}$ current of 100 mA resulted in total trigger rates of about 20 Hz and 70% live-time.

8.3 Data Taking

APEX ran parasitically to the Tevatron collider program. Due to increased background interactions when antiprotons were being produced and stacked in the Accumulator, data was only be taken during quiet periods when a $\overline{p}$ beam was coasting. Such times occurred during the short period before the daily injection of $\overline{p}$s into the Tevatron or when the Main Ring was not running due to maintenance or repair. To take advantage of these times, the main DAQ computer monitored devices in the accelerator complex, and when conditions were ideal, collaborators were automatically paged to ready the detectors for data taking.

APEX collected data from April to July, 1995, in 135 distinct running periods with $\overline{p}$ beam currents in the range 10 – 200 mA, where 1 mA corresponds

to 10^{10} $\overline{p}$s. A total of 30 $\times$ 10^6 events were recorded. Due to the relatively small size of the final data set (20 Gbytes), events were copied to disk in the Andrew File System at FNAL for offline analysis [24]. This enabled fast turn around of event selection and early analysis. Physics results from the APEX experiment are in preparation.

Acknowledgement

We express our gratitude to the Fermilab management, the U.S. Department of Energy and the U.S. National Science Foundation for their generous support of APEX. The technical staff within the Fermilab Accelerator, Research and Computing Divisions and the Physics and Technical Support Sections have played vital roles in supporting the fabrication and installation of the detector and the running of the experiment. We thank the E760 collaboration for the use of the e.m. calorimeter. The contributions of Tanya Baker, Frank Chase, Megan Donohue, Dominic Gooden, John Quackenbush and Art Torosyan to the construction of the scintillating fiber tracker are gratefully acknowledged. The APEX experiment was performed at the Fermi National Accelerator Laboratory, which is operated by Universities Research Association, under contract DE-AC02-76CH03000 with the U.S. Department of Energy.

References

[1] Review of Particle Properties, Phys. Rev. D54 (1996) 562, and references therein.

[2] G. Gabrielse et al., Phys. Rev. Lett. 65 (1990) 1317.

[3] S. Geer et al. (T861 Collaboration), Phys. Rev. Lett. 72 (1994) 1596.

[4] M. A. Hasan et al., Nucl. Instr. and Meth. A 295 (1990) 73.

[5] Varian Ionization Gauge, Model number UHV-24; Varian/Vacuum Products Division, 121 Hartwell Avenue, Lexington, MA 02173, USA.

[6] Inficon RGA Model Quadrex 100, with Electron Multiplier; Inficon Leybold-Heraeus Inc., 6500 Fly Rd., E. Syracuse, NY 13057, USA.

[7] J. Marriner, F. Mills, K.Y. Ng, A.G. Ruggiero, R. Shafer and K. Takayama, "Stability Criterion and Wall Impedance For the Antiproton Accumulator", Pbar Note 422, Fermilab Internal Note (unpublished).

[8] U. Lauströer, U. van Rienen, and T. Weiland, "URMEL and URMEL-T User Guide", Tech. Rep. M-87-03, DESY, 1987 (unpublished).

[9] P. Zhou, P.L. Colestock and S.J. Werkema, "Trapped Ions and Beam Coherent Instability", Pbar Note 536, Fermilab Internal Note (unpublished).

[10] "OPERA-3d Reference Manual", Vector Fields Limited, 24 Bankside, Kidlington, Oxford OX51JE, England.

[11] PS15A acrylic scintillator, Cadillac Plastic and Chemical Company, 1924 Paulina St., Chicago, IL 60622, USA.

[12] POPOP wavelength shifter, Cadillac Plastic and Chemical Company, 1924 Paulina St., Chicago, IL 60622, USA.

[13] Model XP2081B, Amperex Electronic Corporation, 230 Duffy Ave., Hicksville, NY 11802, USA.

[14] FERA ADC Model 4300, LeCroy Corporation, Chestnut Ridge, New York, USA.

[15] GEANT Version 3.21, R. Brun et al., CERN Program Library.

[16] NE America, 7 Deer Park Dr., Suite A2, Monmouth Junction, NJ 08852, USA.

[17] Photomultiplier tube 9902KA, Thorn EMI Electron Tubes Inc., 23 Madison Rd., Fairfield, NJ 07006, USA.

[18] ADC Model 2249, LeCroy Corporation, Chestnut Ridge, New York, USA.

[19] Bicron BCF12 scintillating fiber, Bicron Corporation, 12345 Kinsman Road, Newbury, OH 44065-9677, USA.

[20] Model R4135a, Hamamatsu Corporation, Hamamatsu City, Japan.

[21] R.C. Ball, et al., Nucl. Instr. and Meth. 197 (1982) 371.

[22] V. White, et al., "The VAXONLINE Software System at Fermilab", IEEE Transactions on Nuclear Science, Vol. NS-34, No. 4, Aug. 1987.

[23] B. Joshel, et al., see for example the ICALEPCS Proceedings, Oct. 29 - Nov. 3, 1995, Fermilab.

[24] J. Streets, et al., "Integrating Data Aquisition and Offline Processing Systems for Small Experiments at Fermilab", CHEP95 Proceedings, LAFEX/CBPF, Rio de Janeiro, Brazil, Sept. 18 - 22, 1995.

Figure Captions

1. Side view of the APEX detector.
2. Beam view of the 144-module e.m. calorimeter with an enlarged view of one module.
3. The mean pulse height vs. distance (x) from the WLS plate for a typical calorimeter module with a fit (constant + exponential) to the data points.
4. Pulse height distributions for minimum-ionizing particles incident on a typical calorimeter module within vertical slices (a) close to (2.5 cm) and (b) far from (5.5 cm) the WLS plate. The solid histograms are from GEANT simulation.
5. Two-cluster invariant mass distributions showing the emergence of the π^0 peak with successive cuts.
6. (a) Two-cluster invariant mass distribution in the region of the π^0 peak. The plot shows a Gaussian fit to the data points and the dashed line indicates the true π^0 mass. (b) Two-cluster invariant mass distribution in the region of the η peak. The plot shows a (Gaussian + polynomial background) fit to the data points and the dashed line indicates the true η mass.
7. Beam view of the scintillation counters in the tail catcher.
8. (a) Schematic of one L-shaped module in the scintillating fiber tracker. (b) Layout of the 4 modules which make up a tracking station. (c) Arrangement of the scintillating fibers on the supporting lucite panel.
9. (a) Track residuals from a target-in calibration run. (b) Reconstructed longitudinal target position from a target-in run. (c) Impact parameter at the target's longitudinal position.
10. Layout of one dE/dx scintillation counter plane.
11. Summed pulse height distribution from one dE/dx counter for single track events. The solid histogram shows a GEANT simulation using 37 total photoelectrons per m.i.p. for the two PMTs.
12. Side view of the muon telescope.
13. The four calorimeter quadrants used for triggering.

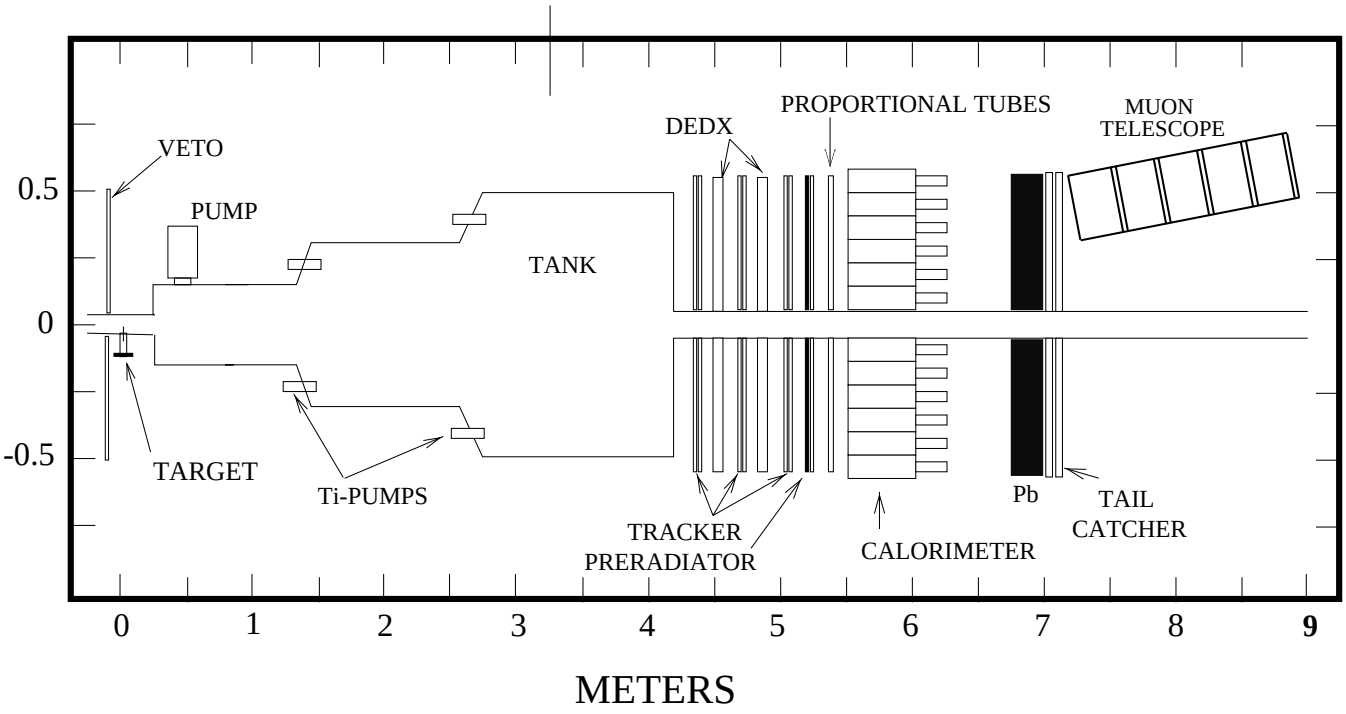

Fig. 1. Side view of the APEX detector

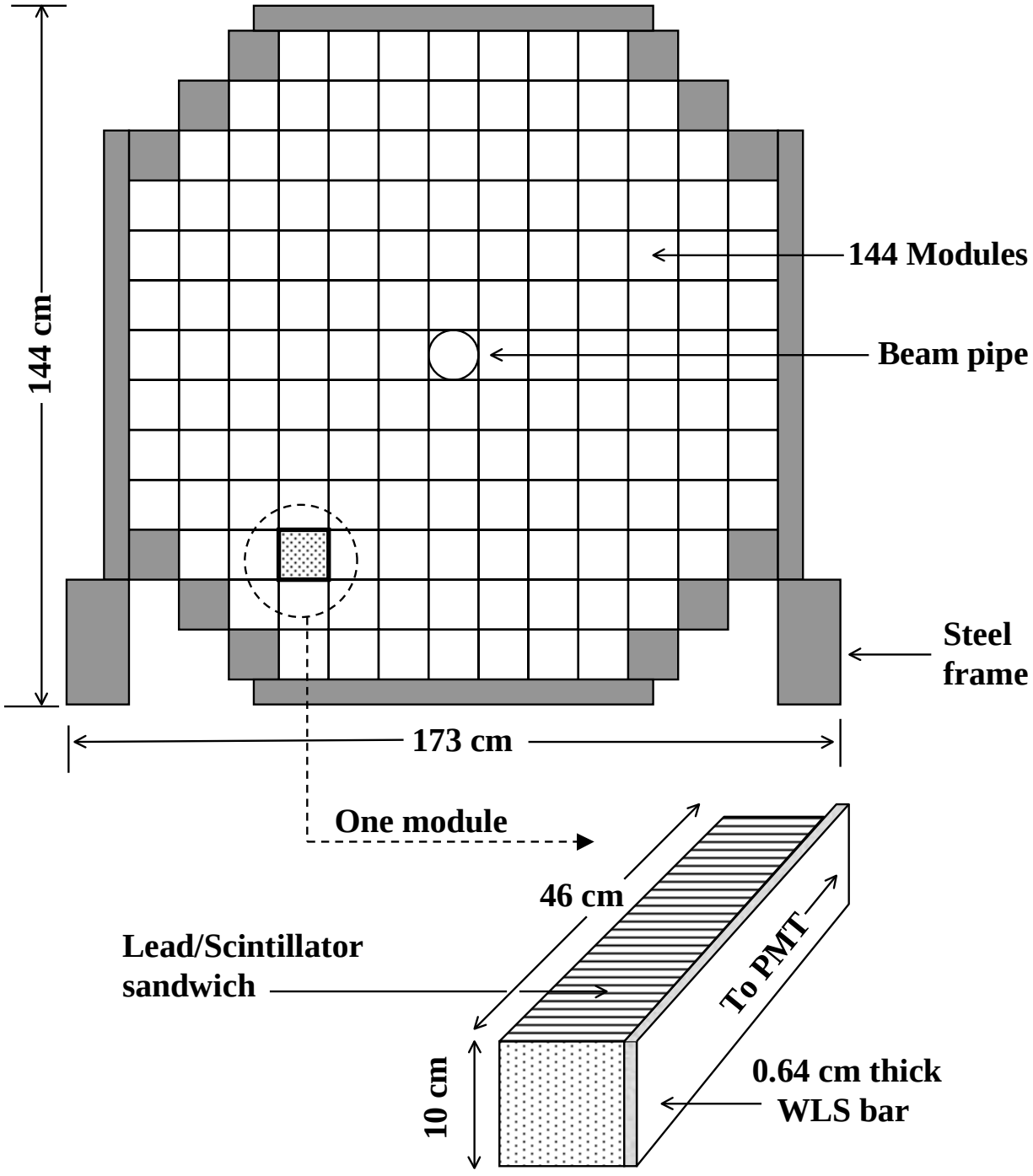

Fig. 2. Beam view of the 144-module e.m. calorimeter with an enlarged view of one module

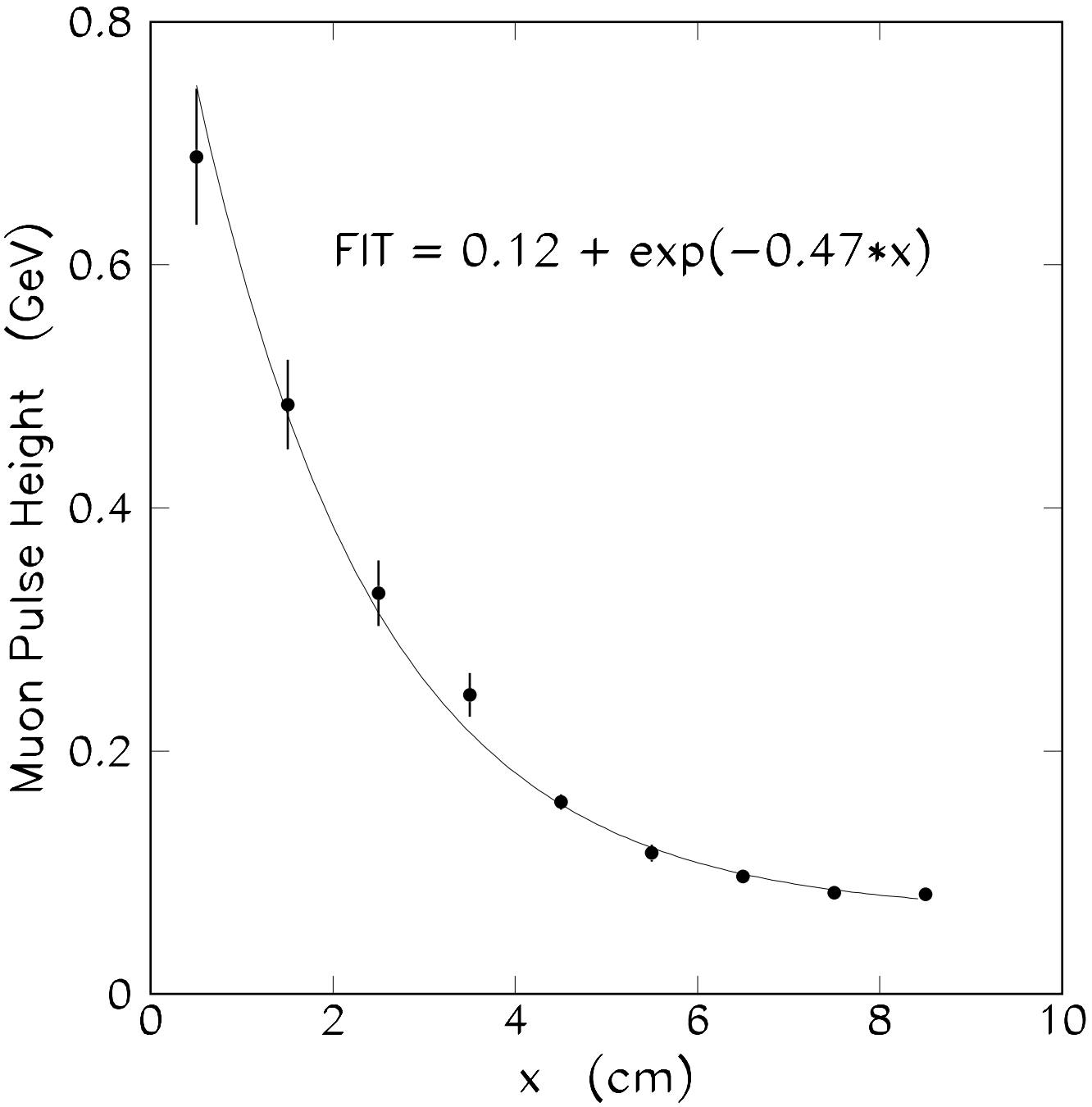

Fig. 3. The mean pulse height vs. distance (x) from the WLS plate for a typical calorimeter module with a fit (constant + exponential) to the data points.

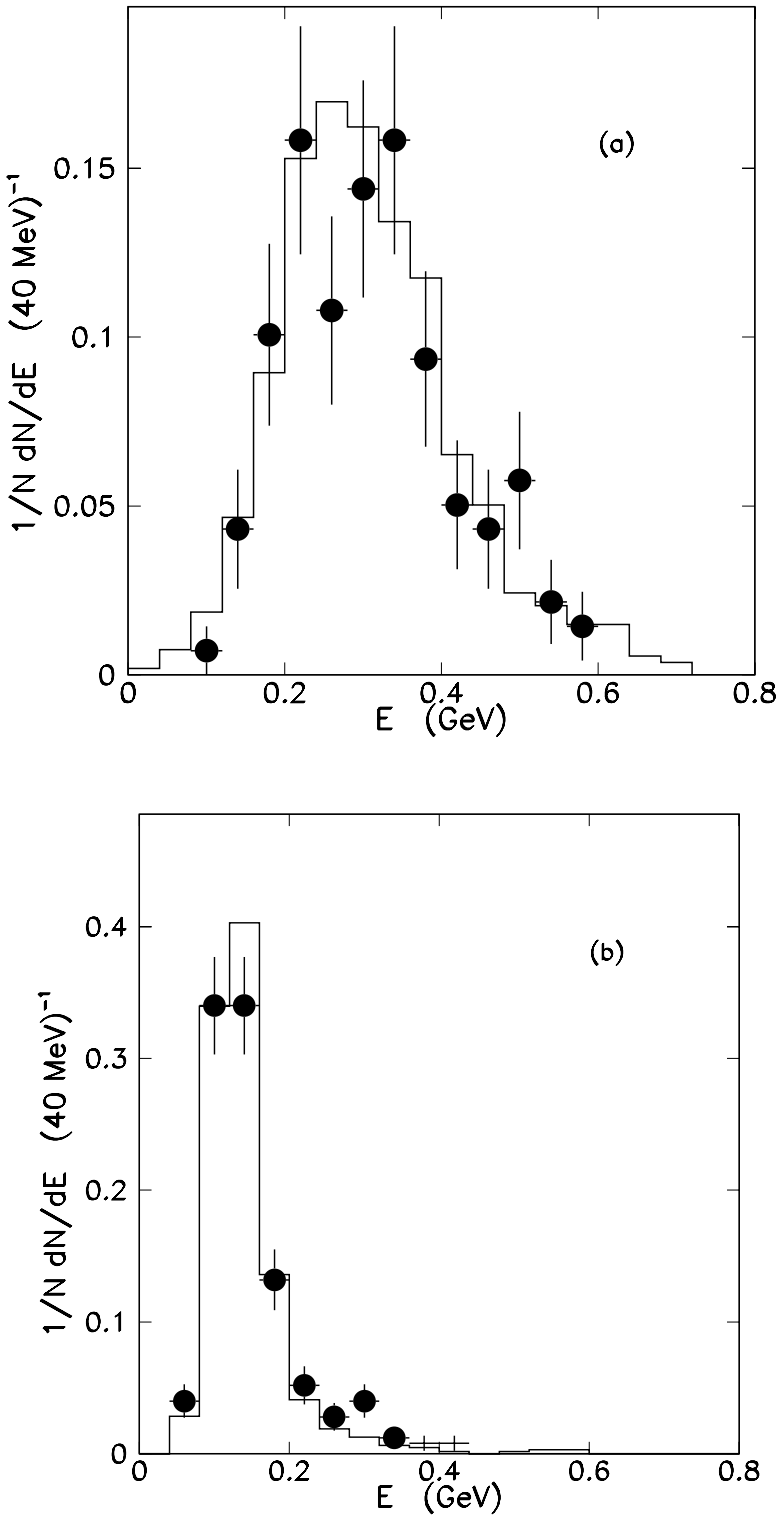

Fig. 4. Pulse height distributions for minimum-ionizing particles incident on a typical calorimeter module within vertical slices (a) close to (2.5 cm) and (b) far from (5.5 cm) the WLS plate. The solid histograms are from GEANT simulation.

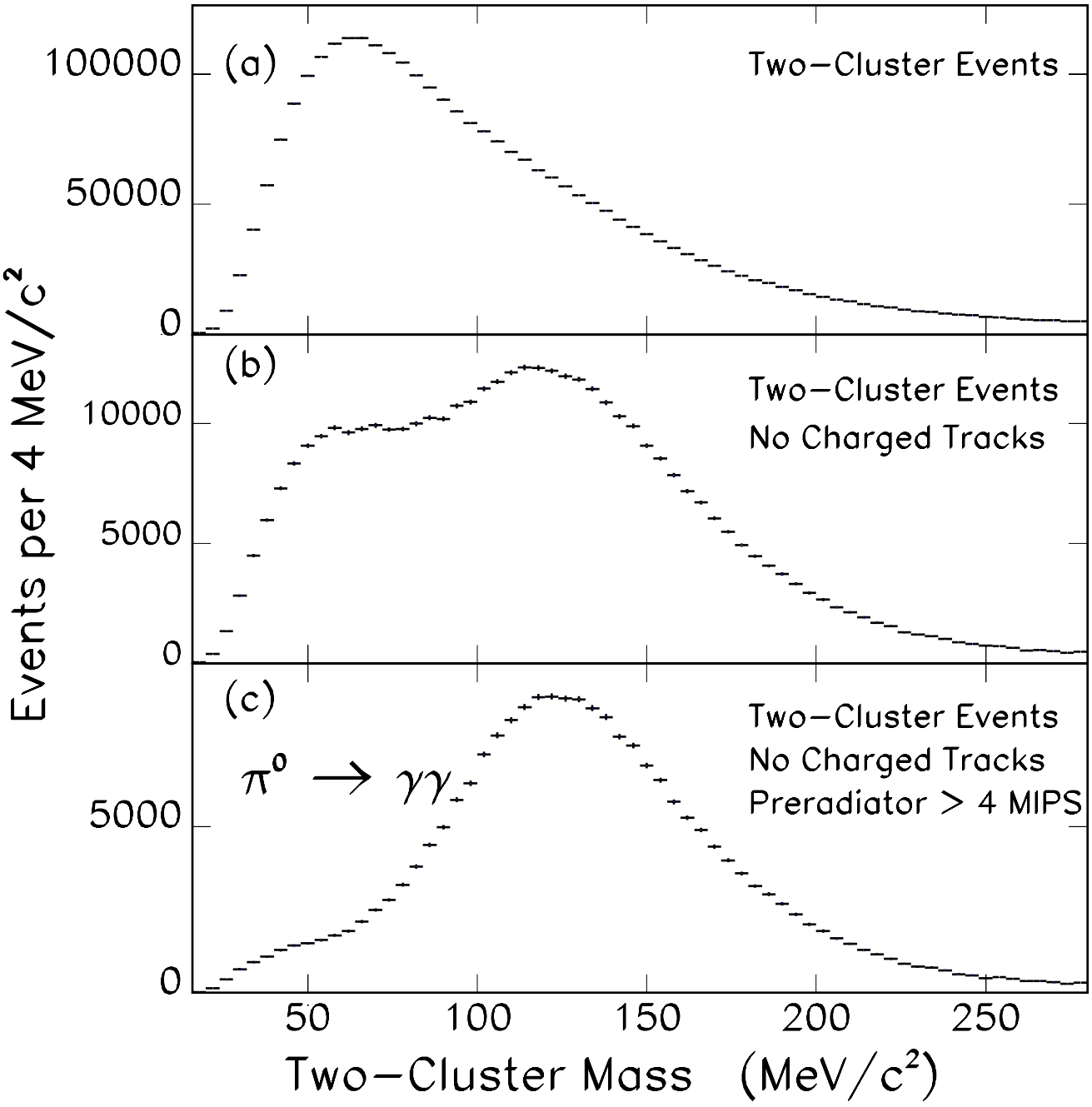

Fig. 5. Two-cluster invariant mass distributions showing the emergence of the π^0 peak with successive cuts.

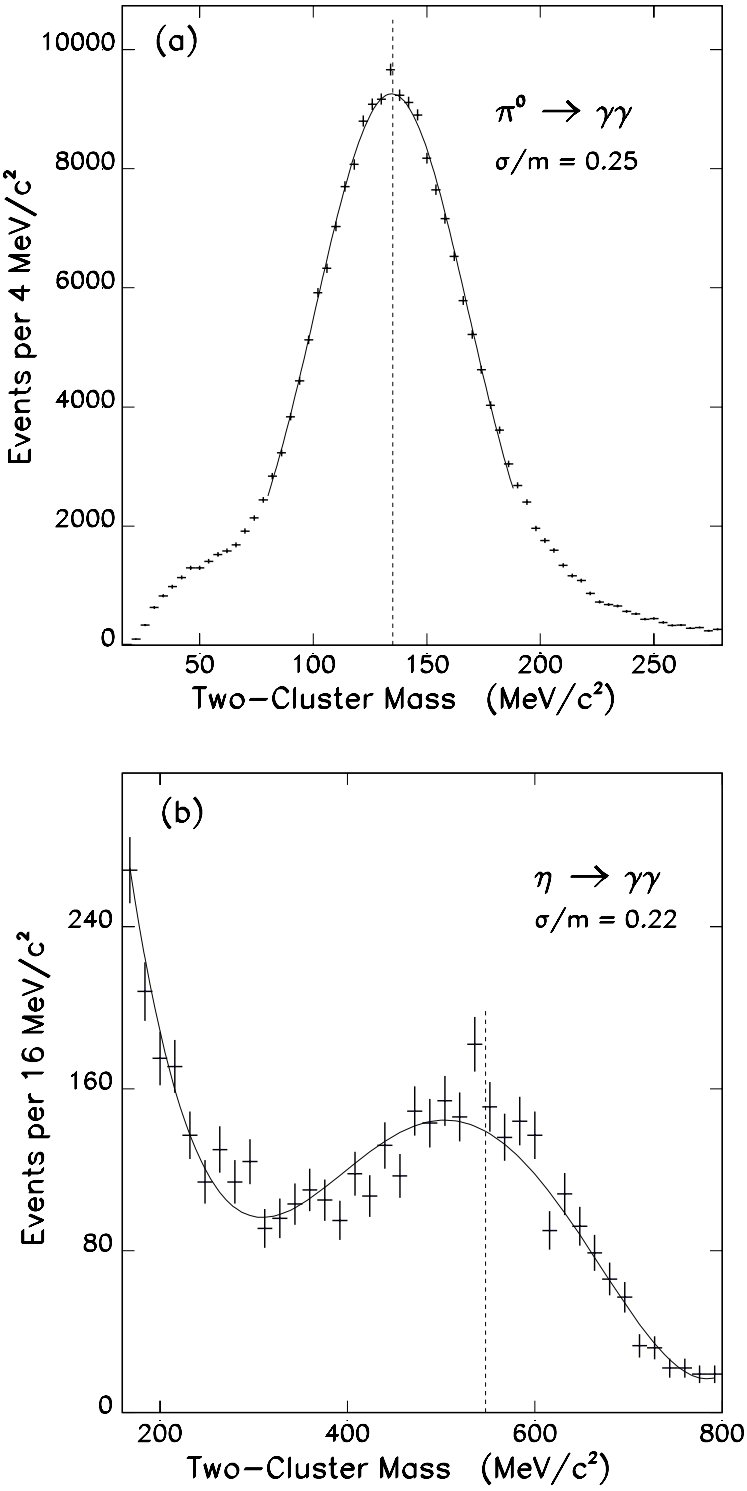

Fig. 6. (a) Two-cluster invariant mass distribution in the region of the π^0 peak. The plot shows a Gaussian fit to the data points and the dashed line indicates the true π^0 mass. (b) Two-cluster invariant mass distribution in the region of the η peak. The plot shows a (Gaussian + polynomial background) fit to the data points and the dashed line indicates the true η mass.

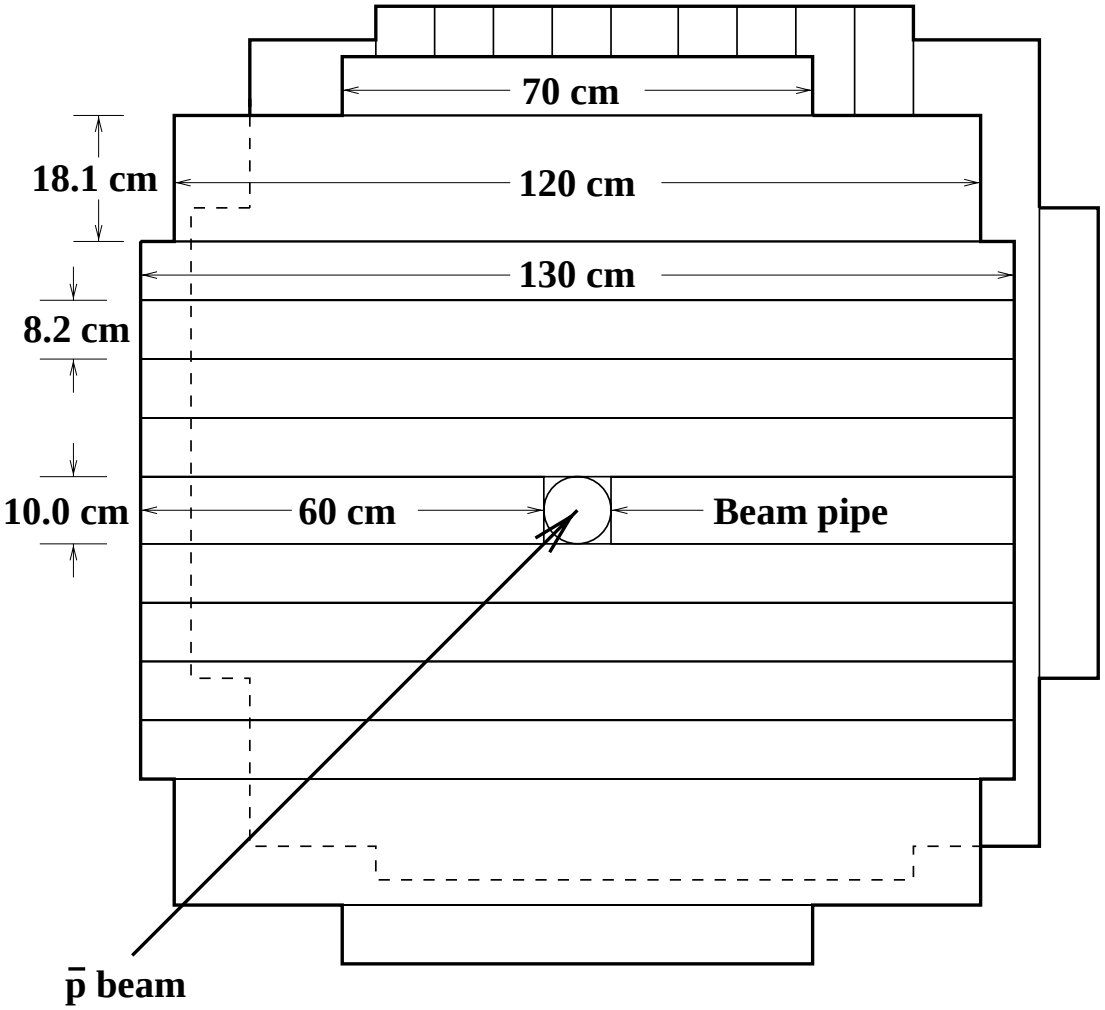

Fig. 7. Beam view of the scintillation counters in the tail catcher.

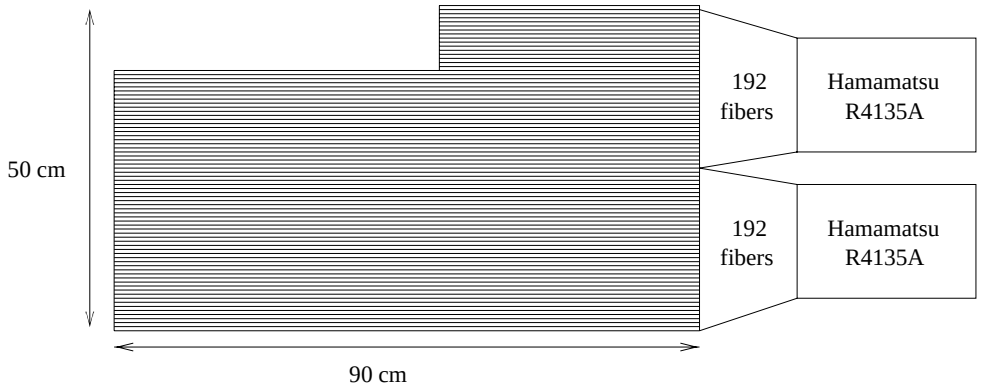

(a)

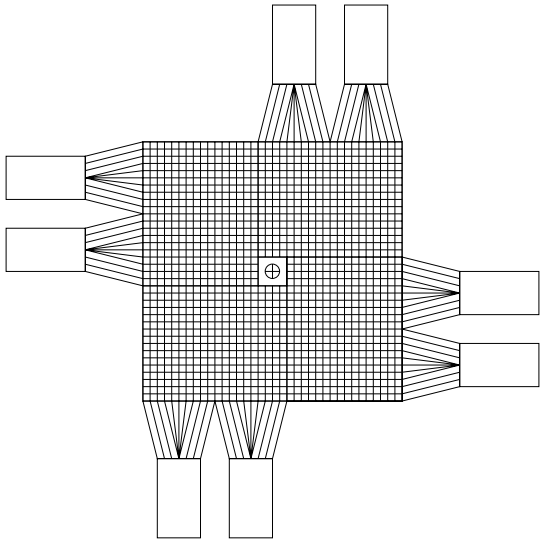

(b)

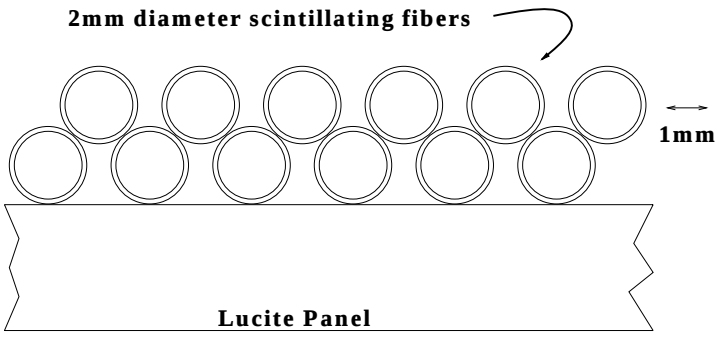

(c)

Fig. 8. (a) Schematic of one L-shaped module in the scintillating fiber tracker. (b) Layout of the 4 modules which make up a tracking station. (c) Arrangement of the scintillating fibers on the supporting lucite panel.

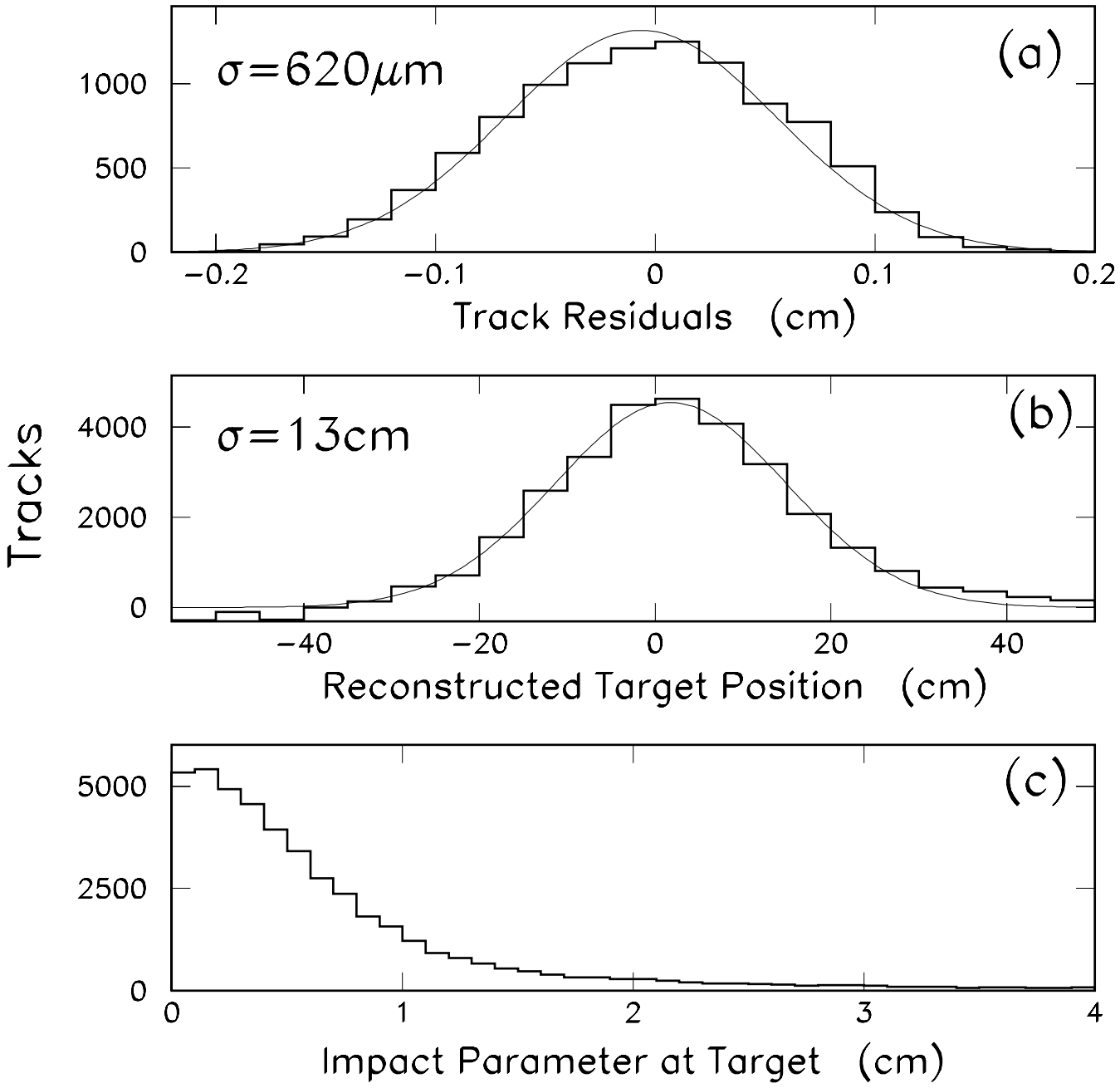

Fig. 9. (a) Track residuals from a target-in calibration run. (b) Reconstructed longitudinal target position from a target-in run. (c) Impact parameter at the target's longitudinal position.

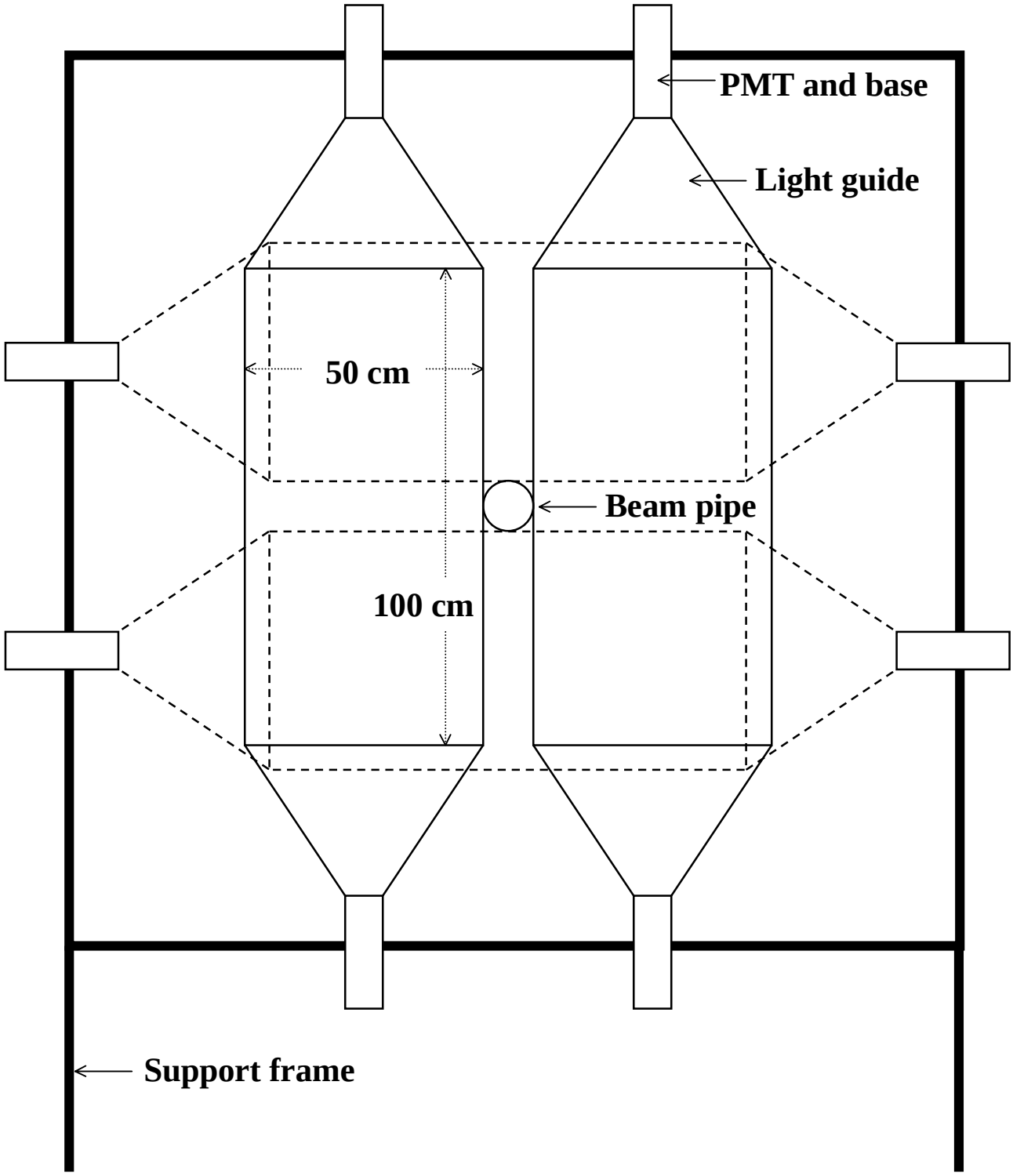

Fig. 10. Layout of one dE/dx scintillation counter plane.

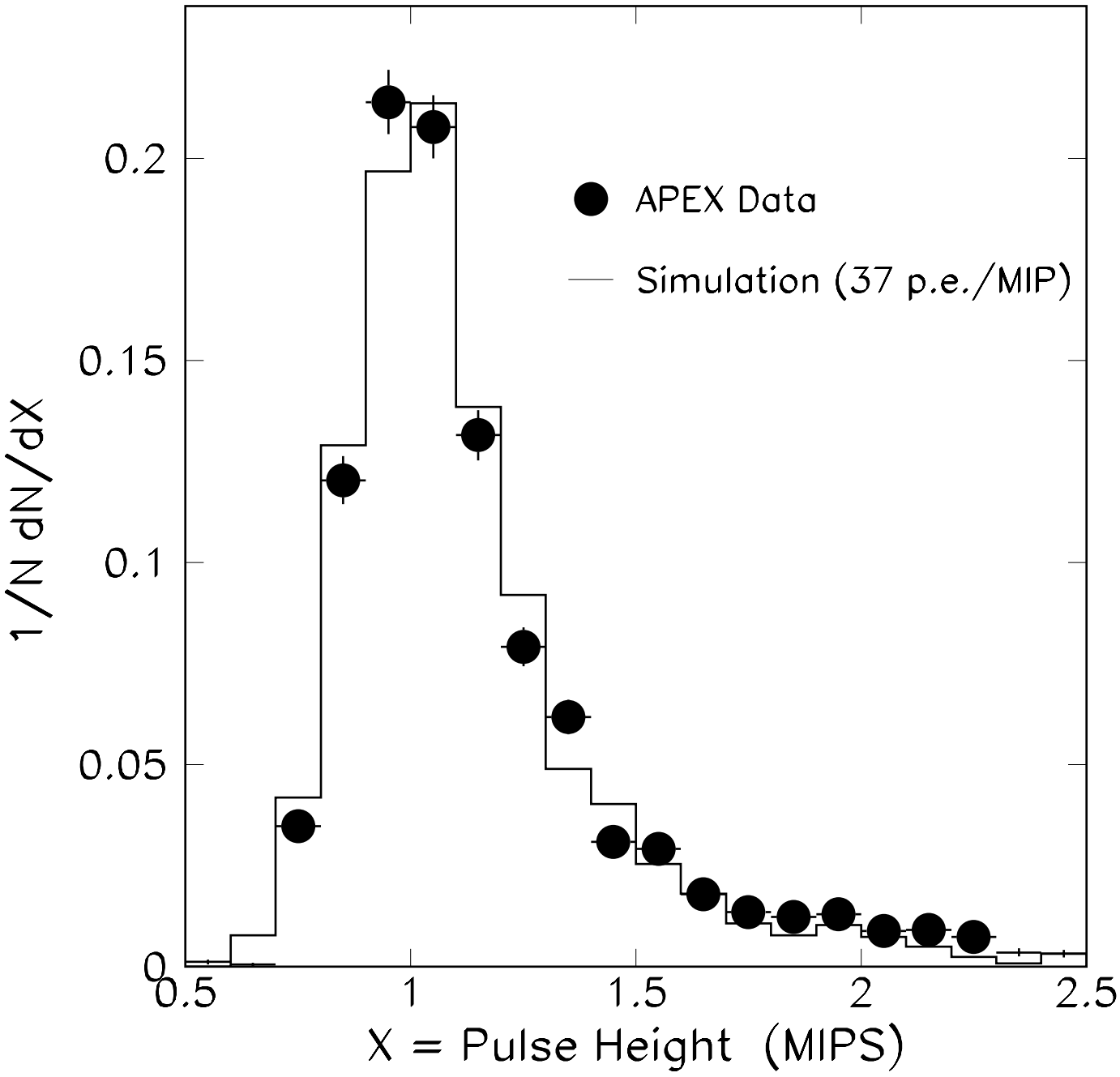

Fig. 11. Summed pulse height distribution from one dE/dx counter for single track events. The solid histogram shows a GEANT simulation using 37 total photoelectrons per m.i.p. for the two PMTs.

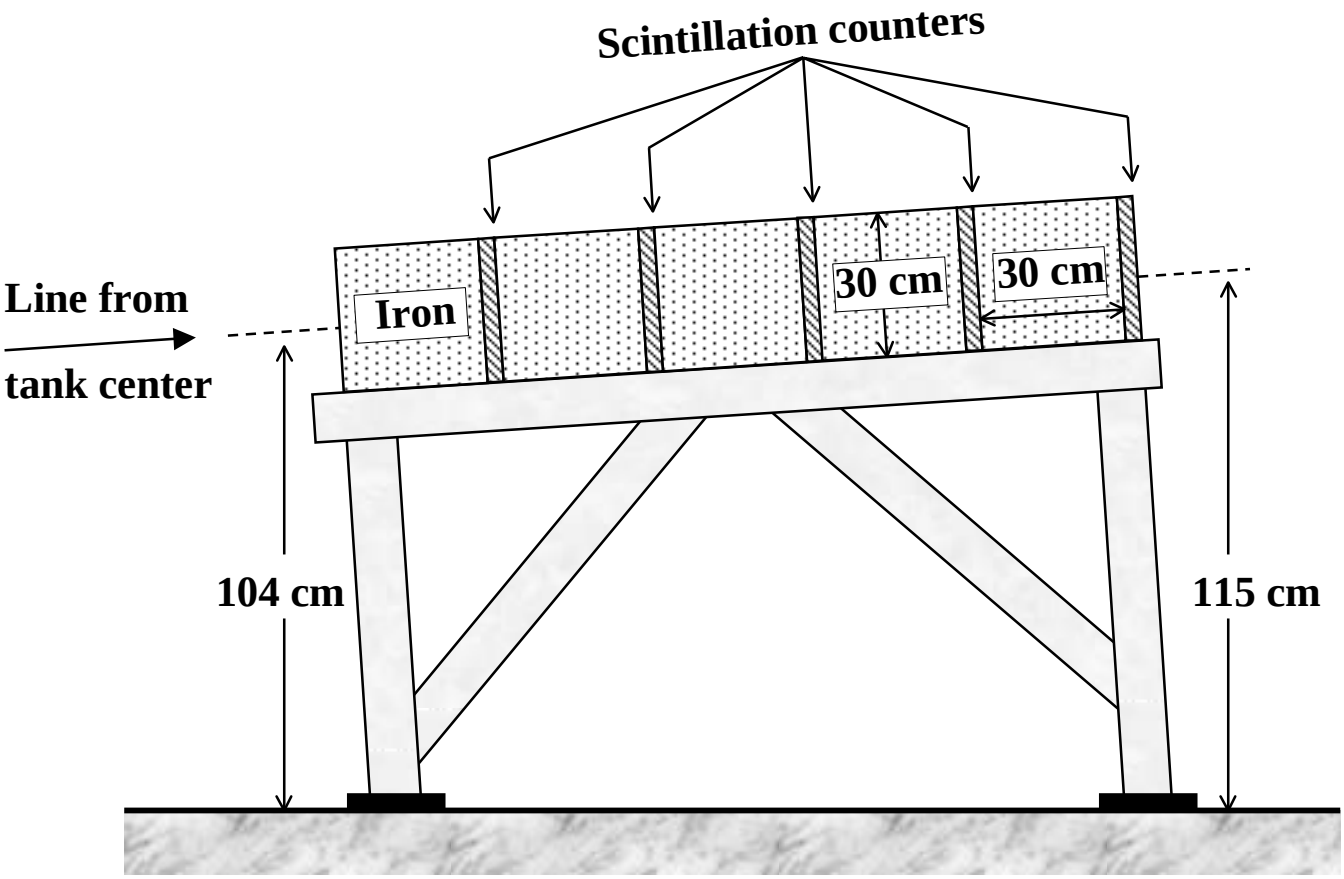

Fig. 12. Side view of the muon telescope.

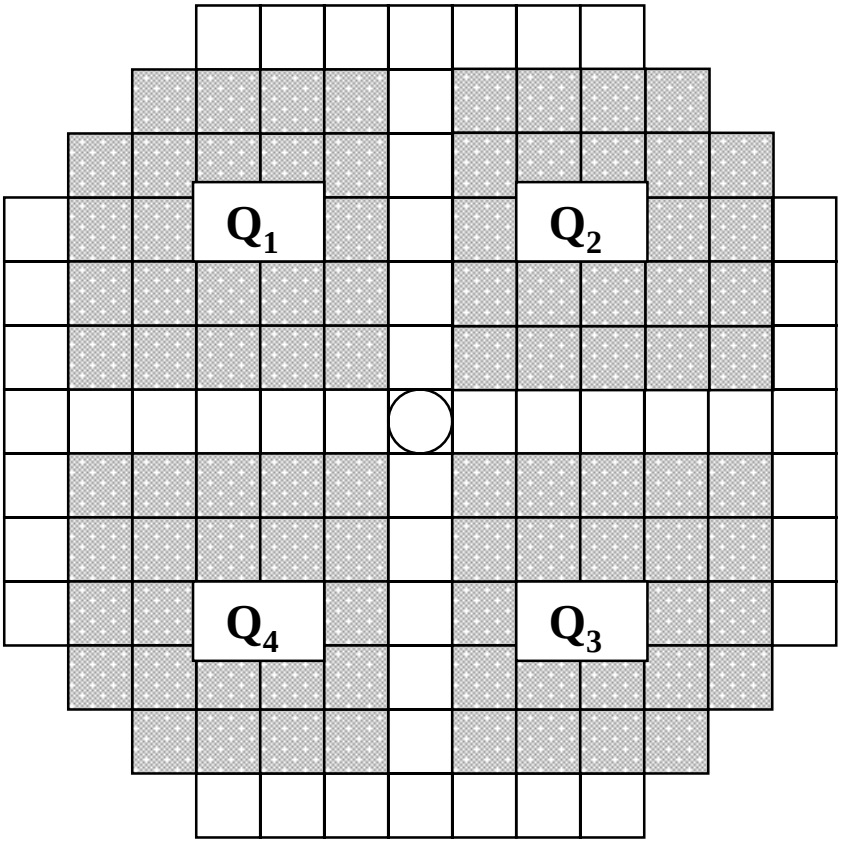

Fig. 13. The four calorimeter quadrants used for triggering.